Mitochondrial energy deficiency leads to hyperproliferation of skeletal muscle mitochondria and enhanced insulin sensitivity

Ryan M. Morrow[a,b], Martin Picard[a,b,1], Olga Derbeneva[a,b,2], Jeremy Leipzig[c], Meagan J. McManus[a,b], Gilles Gouspillou[d], Sébastien Barbat-Artigas[e], Carlos Dos Santos[a,b], Russell T. Hepple[f], Deborah G. Murdock[a,b], and Douglas C. Wallace[a,b,3]

[a]Center for Mitochondrial and Epigenomic Medicine, The Children's Hospital of Philadelphia, Philadelphia, PA 19104; [b]Department of Pathology and Laboratory Medicine, University of Pennsylvania, Philadelphia, PA 19104; [c]Department of Biomedical and Health Informatics, Children's Hospital of Philadelphia, Philadelphia, PA 19104; [d]Département des Sciences de l'Activité Physique, Faculté des Sciences, Université du Québec à Montréal, Montreal, QC, Canada H2L 2C4; [e]Département de Neurosciences, Faculté de Médecine, Université de Montréal, Montreal, QC, Canada H3T 1J4; and [f]Department of Kinesiology, McGill University Health Center, McGill University, Montreal, QC, Canada H3A 0G4

Contributed by Douglas C. Wallace, February 1, 2017 (sent for review June 24, 2016; reviewed by Joseph Bass and Ping H. Wang)

Diabetes is associated with impaired glucose metabolism in the presence of excess insulin. Glucose and fatty acids provide reducing equivalents to mitochondria to generate energy, and studies have reported mitochondrial dysfunction in type II diabetes patients. If mitochondrial dysfunction can cause diabetes, then we hypothesized that increased mitochondrial metabolism should render animals resistant to diabetes. This was confirmed in mice in which the heart–muscle–brain adenine nucleotide translocator isoform 1 (ANT1) was inactivated. ANT1-deficient animals are insulin-hypersensitive, glucose-tolerant, and resistant to high fat diet (HFD)-induced toxicity. In ANT1-deficient skeletal muscle, mitochondrial gene expression is induced in association with the hyperproliferation of mitochondria. The ANT1-deficient muscle mitochondria produce excess reactive oxygen species (ROS) and are partially uncoupled. Hence, the muscle respiration under nonphosphorylating conditions is increased. Muscle transcriptome analysis revealed the induction of mitochondrial biogenesis, down-regulation of diabetes-related genes, and increased expression of the genes encoding the myokines FGF21 and GDF15. However, FGF21 was not elevated in serum, and FGF21 and UCP1 mRNAs were not induced in liver or brown adipose tissue (BAT). Hence, increased oxidation of dietary-reducing equivalents by elevated muscle mitochondrial respiration appears to be the mechanism by which ANT1-deficient mice prevent diabetes, demonstrating that the rate of mitochondrial oxidation of calories is important in the etiology of metabolic disease.

mitochondria | skeletal muscle | ANT1 | insulin sensitivity

Multiple studies suggest that human diabetes and insulin resistance are accompanied by impaired mitochondrial oxidative metabolism. Studies of patients with type II diabetes have revealed that mitochondrial gene expression is generally down-regulated. In particular, the mitochondrial biogenesis transcription factor PGC-1α and its downstream transcriptional targets are lower in diabetics compared with controls (1–4); the enzymatic activity of NADH dehydrogenase (complex I) is reduced by 40% in skeletal muscle biopsies from obese, insulin-resistant individuals (5); mitochondrial size is diminished in obesity and diabetes (5, 6); ADP-stimulated respiration is reduced in permeabilized muscle fibers from obese, diabetic individuals (7, 8); and skeletal muscle, which accounts for >80% of insulin-stimulated glucose disposal, has impaired mitochondrial oxidative phosphorylation (OXPHOS) in diabetics (9, 10). Mitochondrial DNA (mtDNA) rearrangements (11, 12) and $tRNA^{Leu(UUR)}$ nucleotide (nt) 3243A > G (13) mutations have been linked to diabetes, and the $tRNA^{Ile}$ nt 4291T > C mutation has been associated with metabolic syndrome (14).

In mitochondrial myopathy, muscle mitochondrial stress is associated with the induction of the myokines fibroblast growth factor 21 (FGF21) (15, 16) and growth differentiation factor 15 (GDF15) (17). Elevated FGF21 and GDF15 are associated with diabetes and glucose intolerance (18, 19) but have been shown to reduce serum glucose and insulin levels (20). Elevated FGF21 can act non-cell autonomously to induce uncoupling protein 1 (UCP1) in brown adipose tissue (BAT), resulting in increased mitochondrial oxidation of lipids (21).

The mitochondrial inner membrane adenine nucleotide translocators (ANTs) exchange mitochondrial ATP for cytosolic ADP. The mouse has two major somatic ANT isoforms: ANT1, which is predominantly expressed in heart, muscle, and brain; and ANT2, which is expressed in all tissues except muscle (22). Mice in which the ANT1 gene is deleted develop mitochondrial myopathy in association with the hyperproliferation of skeletal muscle mitochondria (23, 24).

Here we demonstrate that $Ant1^{-/-}$ mice have a striking resistance to the metabolic toxicity of a high fat diet (HFD). This is associated with excessive proliferation of partially uncoupled skeletal muscle

Significance

Mitochondrial dysfunction is associated with type II diabetes and metabolic syndrome, but whether it is cause or consequence is debated. By showing that increased mitochondrial respiration can impart glucose tolerance, insulin sensitivity, and resistance to high fat diet (HFD) toxicity, we provide evidence that mitochondria contributes to the etiology of metabolic disease. Inactivation of adenine nucleotide translocator isoform 1 (ANT1) results in proliferation of partially uncoupled muscle mitochondrial respiration, creating a sink for excess calories. Although ANT1-deficient muscle induces expression of *Fgf21*, FGF21 level is not elevated in blood, and FGF21 and UCP1 mRNAs are not increased in liver or brown adipose tissue (BAT). If increased mitochondrial respiration prevents HFD toxicity, then decreased mitochondrial respiration may contribute to metabolic disease.

Author contributions: R.M.M., M.P., R.T.H., and D.C.W. designed research; R.M.M., M.P., O.D., M.J.M., G.G., S.B.-A., C.D.S., and D.G.M. performed research; R.M.M., M.P., J.L., G.G., and D.G.M. analyzed data; and R.M.M., D.G.M., and D.C.W. wrote the paper.

Reviewers: J.B., Northwestern University Medical School; and P.H.W., University of California, Irvine.

The authors declare no conflict of interest.

Freely available online through the PNAS open access option.

[1]Present address: Division of Behavioral Medicine, Department of Psychiatry, Department of Neurology, Columbia Translational Neuroscience Initiative, Columbia University College of Physicians and Surgeons, Columbia University Medical Center, New York, NY 10032.

[2]Present address: Research and Operations, DxTerity Diagnostics, Rancho Dominguez, CA 90220.

[3]To whom correspondence should be addressed. Email: wallaced1@email.chop.edu.

This article contains supporting information online at www.pnas.org/lookup/suppl/doi:10.1073/pnas.1700997114/-/DCSupplemental.

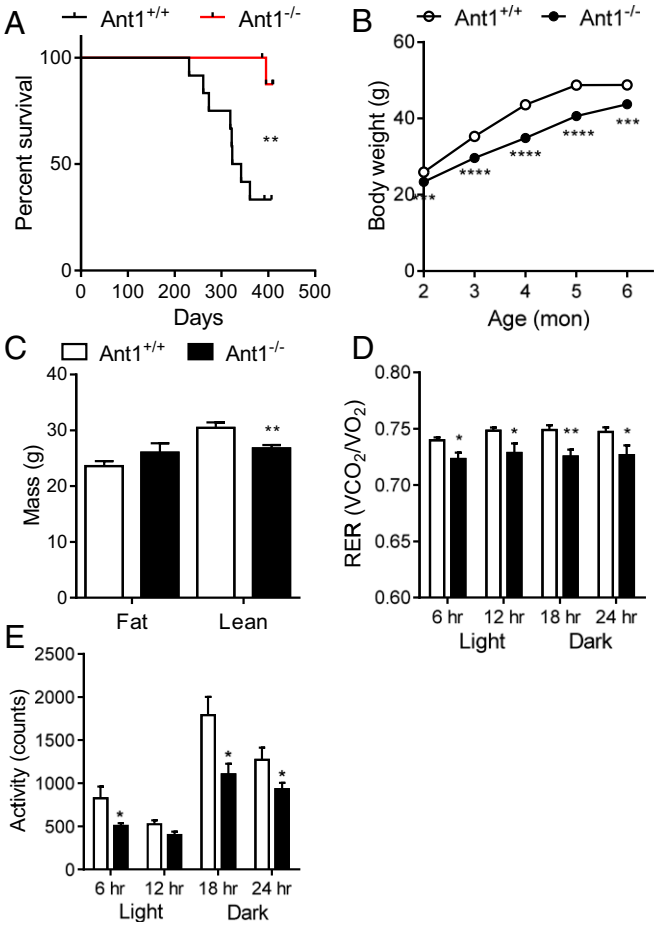

Fig. 1. ANT1 deficiency provides resistance to HFD and modulates metabolism. (*A*) Kaplan–Meier survival curve of $Ant1^{+/+}$ and $Ant1^{-/-}$ mice fed a HFD. (*B*) Body weight measured in mice fed a HFD. (*C*) Body composition measured by MRI in 8-mo-old mice fed a HFD. (*D*) RER measured over 24 h in 8–9-mo-old mice fed a HFD. (*E*) Activity levels measured over 24 h in 8–9-mo-old mice fed a HFD. Data are represented as mean ± SEM; n = 10–12 per group (*A*), 16–28 per group (*B*), and 6–9 per group (*C*–*E*). *$P < 0.05$; **$P < 0.01$; ***$P < 0.001$; ****$P < 0.0001$.

mitochondria resulting in higher than normal muscle respiration levels. Although FGF21 and GDF15 mRNAs are induced in muscle, FGF21 is not elevated in blood nor are FGF21 or UCP1 mRNAs induced in liver or BAT. Hence, in $Ant1^{-/-}$ mice, the high degree of insulin sensitivity, glucose tolerance, and resistance to HFD toxicity appears to be the result of the oxidation of excess carbohydrates and fats in the muscle mitochondria.

Results

Protection from HFD Toxicity in ANT1-Deficient Mice. $Ant1^{-/-}$ mice are markedly resistant to the toxicity of a HFD surviving past 1 y, a timepoint at which 75% of the $Ant1^{+/+}$ mice had already died (Fig. 1*A*). On a low fat diet (LFD) $Ant1^{-/-}$ mice show a slight reduction in survival (Fig. S1*A*). $Ant1^{-/-}$ mice have a 17% and 12% lower body weight than $Ant1^{+/+}$ mice on a HFD (Fig. 1*B*) and LFD (Fig. S1*B*), respectively. Because they have similar levels of fat mass on the two diets as evaluated by NMR, the weight difference must reside in a reduction of lean mass on HFD (Fig. 1*C*) and LFD (Fig. S1*C*).

In 8–9-mo-old $Ant1^{-/-}$ mice housed in metabolic cages on a HFD, there is a slight decrease in the respiratory exchange ratio (RER; VCO_2/VO_2), indicating a greater reliance on lipid substrates than glycolytic substrates (Fig. 1*D*). The LFD shifts this relationship, such that there is a 6% increase in RER in the $Ant1^{-/-}$ mice during the first 6 h of the dark cycle, indicating a greater reliance on glycolytic substrates and greater metabolic flexibility (Fig. S1*D*).

The $Ant1^{-/-}$ mice on a HFD are 39% less active than $Ant1^{+/+}$ mice during the first 6 h of the light cycle and ∼33% less active during both 6-h phases of the dark cycle (Fig. 1*E*). $Ant1^{-/-}$ mice on a LFD have a similar 36% decrease in activity during the light phase and a 45% decrease across both dark phases (Fig. S1*E*). Despite decreased activity, there was no difference in O_2 consumption or food intake between $Ant1^{-/-}$ and $Ant1^{+/+}$ on either diet (Fig. S1 *F*–*H*). Therefore, for the same amount of activity, the $Ant1^{-/-}$ mice must consume more calories.

ANT1 Deficiency Promotes Glucose Tolerance and Insulin Sensitivity. The fasting blood glucose levels of 9-mo-old $Ant1^{+/+}$ and $Ant1^{-/-}$ on a HFD (Fig. 2*A*) and 24-mo-old $Ant1^{+/+}$ and $Ant1^{-/-}$ mice on a LFD (Fig. S2*A*) showed no differences and fell within the euglycemic range of 60–120 mg/dL. However, the $Ant1^{-/-}$ mice have a 45% and 24% reduction in fasting plasma insulin levels on HFD (Fig. 2*B*) and LFD (Fig. S2*B*), respectively, indicating the $Ant1^{+/+}$ mice develop age-related and diet-induced insulin resistance while the $Ant1^{-/-}$ mice are protected.

When subjected to an i.p. glucose tolerance test (IPGTT), the $Ant1^{-/-}$ mice showed faster glucose clearance than $Ant1^{+/+}$ mice when maintained on either the HFD (Fig. 2*A*) or LFD (Fig. S2*A*). During the IPGTT, the plasma insulin levels were 40–50% lower in $Ant1^{-/-}$ mice maintained on both HFD (Fig. 2*B*) and LFD (Fig. S2*B*). Thus, better glucose clearance was achieved in the $Ant1^{-/-}$ mice with minimal secretion of insulin. This data suggest that first-phase insulin secretion was nearly absent in the $Ant1^{-/-}$ pancreas, though *Ant1* is not expressed in the pancreas or liver (22).

For mice maintained on a HFD for 8–9 mo, subjection to a hyperinsulinemic–euglycemic clamp revealed that during hyperinsulinemia, $Ant1^{-/-}$ mice had a 16% increase in the rate of glucose disposal (Rd) and their glucose infusion rate (GIR) was 65%

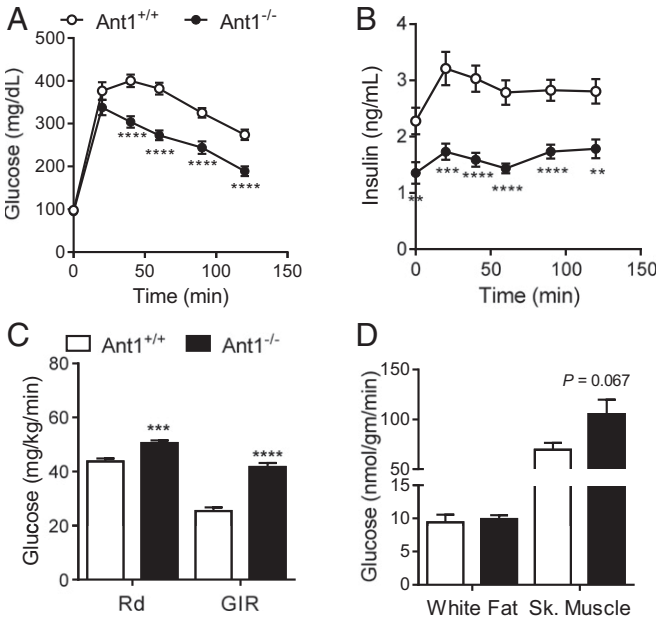

Fig. 2. ANT1 deficiency enhances insulin sensitivity. (*A*) Glucose tolerance test performed in 9-mo-old mice fed a HFD for 6 mo. (*B*) Plasma insulin levels during the glucose tolerance test. (*C*) Hyperinsulinemic–euglycemic clamp performed on 8–9-mo-old mice fed a HFD. GIR, glucose infusion rate; Rd, rate of glucose disposal. (*D*) ^{14}C-2-deoxyglucose uptake in white fat and skeletal muscle. Data are represented as mean ± SEM; n = 16–28 per group (*A* and *B*) and 7–9 per group (*C* and *D*). **$P < 0.01$; ***$P < 0.001$; ****$P < 0.0001$.

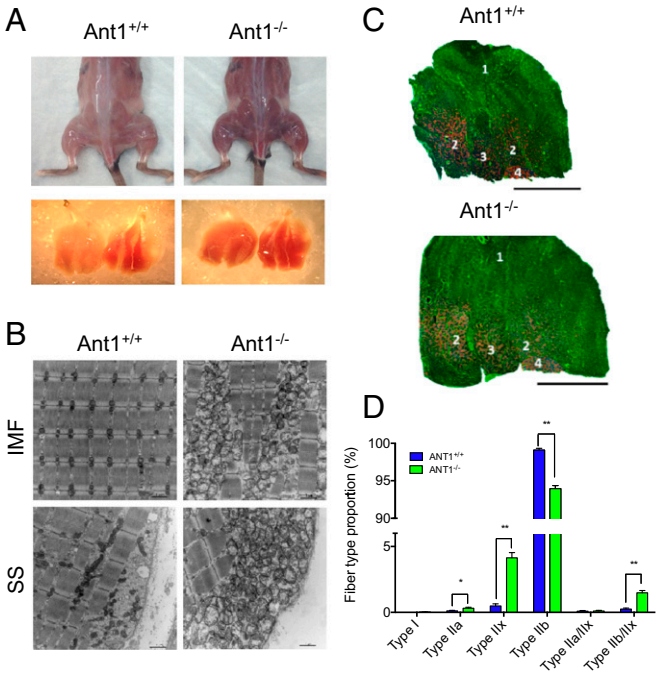

Fig. 3. Skeletal muscle morphology in Ant1$^{-/-}$ mice. *Ant1*$^{+/+}$ and *Ant1*$^{-/-}$ mice fed a HFD were killed at 12 mon. *Ant1*$^{-/-}$ mice show increased reddening in (*A*) whole-body skeletal muscle and isolated gastrocnemius. (*B*) Representative electron micrographs of white gastrocnemius in the intermyofibrillar (IMF) and subsarcolemmal (SS) compartments. (*C*) Representative triple MHC labeling (MHCI, blue; MHCIIa, red; MHCIIb, green; MHCIIx, black) performed in *Ant1*$^{+/+}$ and *Ant1*$^{-/-}$ mice. (Scale bar, 2,000 μm.). 1, white gastrocnemius; 2, red gastrocnemius; 3, plantaris; 4, soleus. (*D*) Fiber type proportion in white gastrocnemius from *Ant1*$^{+/+}$ and *Ant1*$^{-/-}$ mice. Data are represented as mean ± SEM; $n = 2$ per group. *$P < 0.01$; **$P < 0.01$.

higher than those of *Ant1*$^{+/+}$ mice (Fig. 2*C*). The *Ant1*$^{-/-}$ mice on a LFD had a 48% higher Rd and a 65% higher GIR, revealing that *Ant1*$^{-/-}$ mice are more insulin-sensitive (Fig. S2*C*).

To measure glucose uptake ^{14}C-2-deoxyglucose was injected into the mice during the hyperinsulinemic–euglycemic clamp. The white fat and skeletal muscle were removed from the animals, and the radiolabeled glucose in these tissues was counted. On a HFD, the *Ant1*$^{-/-}$ mice displayed a trend of increased glucose uptake in the skeletal muscle (Fig. 2*D*). On a LFD, *Ant1*$^{-/-}$ mice had 70% more glucose uptake in the white adipose tissue (WAT) than the *Ant1*$^{+/+}$ mice but no difference in skeletal muscle uptake (Fig. S2*D*).

Mitochondrial Proliferation in Skeletal Muscle. To assess the effects of the ANT1 defect on the skeletal muscle mitochondria, we isolated whole gastrocnemius from 12-mo-old *Ant1*$^{+/+}$ and *Ant1*$^{-/-}$ mice fed a HFD. At the macroscopic level, the *Ant1*$^{-/-}$ mice had darker skeletal muscle tissue, indicative of mitochondrial proliferation (25) (Fig. 3*A*). The gastrocnemius muscle, which is composed of glycolytic (white) and oxidative (red) fibers, was redder in the *Ant1*$^{-/-}$ mouse.

Ultrastructural analysis by transmission electron microscopy revealed hyperproliferation of swollen mitochondria with disordered cristae in the *Ant1*$^{-/-}$ mouse muscle. The intermyofibrillar compartment of the *Ant1*$^{+/+}$ mice have an ordered array of mitochondria with dense mitochondrial matrix along the Z-lines of the sarcomeres, whereas the *Ant1*$^{-/-}$ mice exhibited hyperproliferation of abnormal mitochondria, which displaced the myofibrils (Fig. 3*B*). Similarly, in the subsarcolemmal compartment, the *Ant1*$^{+/+}$ mice have a normal number of dense mitochondria, whereas the *Ant1*$^{-/-}$ mice have numerous swollen mitochondria (Fig. 3*B*).

To determine if the reddening of the *Ant1*$^{-/-}$ muscle was due to conversion of glycolytic fibers into oxidative fibers, we analyzed cryosections for myosin heavy chain (MHC) isoforms type I, IIa, IIb, and IIx by immunohistochemistry (Fig. 3*C*). In the *Ant1*$^{-/-}$ white gastrocnemius muscle, there was an increase in oxidative type IIa, type IIx, and coexpressing type IIb/IIx fibers and a decrease in glycolytic type IIb fibers (Fig. 3*D*). Hence, ANT1 deficiency caused a partial shift to more oxidative myofiber phenotypes.

***Ant1*$^{-/-}$ Muscle Fiber Biochemistry.** The striking resistance of *Ant1*$^{-/-}$ mice to the toxicity of a HFD, together with the hyperproliferation of mitochondria, which oxidize pyruvate and fatty acids, suggests that the excess mitochondria may be protecting the mice from calorie overload. Consistent with this hypothesis, in 12-mo-old *Ant1*$^{-/-}$ and *Ant1*$^{+/+}$ mice fed a HFD, the citrate synthase (CS), cytochrome *c* oxidase (COX, complex IV), and succinate dehydrogenase (SDH, complex II) activity levels per mg muscle protein were increased four- to sevenfold in white *Ant1*$^{-/-}$ gastrocnemius (Fig. 4 *A*–*C*) and three- to fourfold in the red *Ant1*$^{-/-}$ gastrocnemius (Fig. S3 *A*–*C*). Relative mtDNA content was increased two- to fourfold in white (Fig. 4*D*) and red (Fig. S3*D*) gastrocnemius, respectively.

To assess mitochondrial function, bundles of white and red muscle fibers were dissected from the gastrocnemius, permeabilized with saponin, and the mitochondrial respiration was measured. The sequential addition of glutamate and malate (G/M, complex I substrates), ADP, and succinate (Succ, complex II substrate) revealed an approximate 60% and 80% reduction in state II and III respiration in *Ant1*$^{-/-}$ versus *Ant1*$^{+/+}$ white and red muscle fibers when values were normalized by the specific activity of CS, indicative of activity per individual mitochondrion (Fig. 4*E* and Fig. S3*E*). These observations are consistent with limited ADP/ATP exchange due to the ANT1 deficiency.

However, when the G/M (complex I) respiration rates were normalized to muscle wet weight, the state II respiration rate, which represents respiration not linked to ATP synthesis, was increased in the *Ant1*$^{-/-}$ muscle by 161% for white fibers (Fig. 4*F*) and 57% for red fibers (Fig. S3*F*). When metabolizing G/M in the presence of ADP, the respiration rate was 14% lower in the *Ant1*$^{-/-}$ white muscle fibers and 31% lower in the *Ant1*$^{-/-}$ red muscle fibers, consistent with ANT1 deficiency inhibiting ADP import into the mitochondrion. However, when metabolizing both G/M and Succ in the presence of ADP (complex I and II), respiration per unit of muscle was 35% higher in *Ant1*$^{-/-}$ white muscle fibers compared with *Ant1*$^{+/+}$ (Fig. 4*F*) and not significantly different between the *Ant1*$^{-/-}$ and *Ant1*$^{+/+}$ red muscle fibers (Fig. S3*F*).

Finally, in the *Ant1*$^{-/-}$ muscle, the respiratory control ratio (RCR, state III/state II respiration) was 56% and 67% of *Ant1*$^{+/+}$ in white and red muscle fibers, respectively, consistent with the electron transport chain being partially uncoupled from ATP synthesis (Fig. S3 *G* and *H*). The exact molecular mechanism for this apparent "uncoupling" is unknown, as it could result from nonspecific leak across the inner membrane, flickering of the mtPTP, or some other mechanism. However, the result is that the increased mitochondrial mass and the decoupling of mitochondrial OXPHOS from limiting ATP synthesis in the *Ant1*$^{-/-}$ muscle more than offsets the respiratory defect resulting from impaired ADP/ATP exchange of the *Ant1*$^{-/-}$ mitochondria, a result consistent with the increased oxygen consumption in *Ant1*$^{-/-}$ mice.

To assess the effect of ANT1 deficiency on muscle mitochondrial ROS production, mitochondrial H_2O_2 production was quantified in permeabilized myofibers using Amplex Red, during the sequential addition of G/M, Succ, ADP, and antimycin a (AA). When metabolizing G/M, and normalized to CS, H_2O_2 production was reduced 81% in *Ant1*$^{-/-}$ white fibers (Fig. 4*G*) and 67% in *Ant1*$^{-/-}$ red fibers (Fig. S3*I*). When metabolizing Succ, H_2O_2 production was reduced by 53% and 43% in white and red fibers. When metabolizing G/M, Succ, and ADP, H_2O_2 production

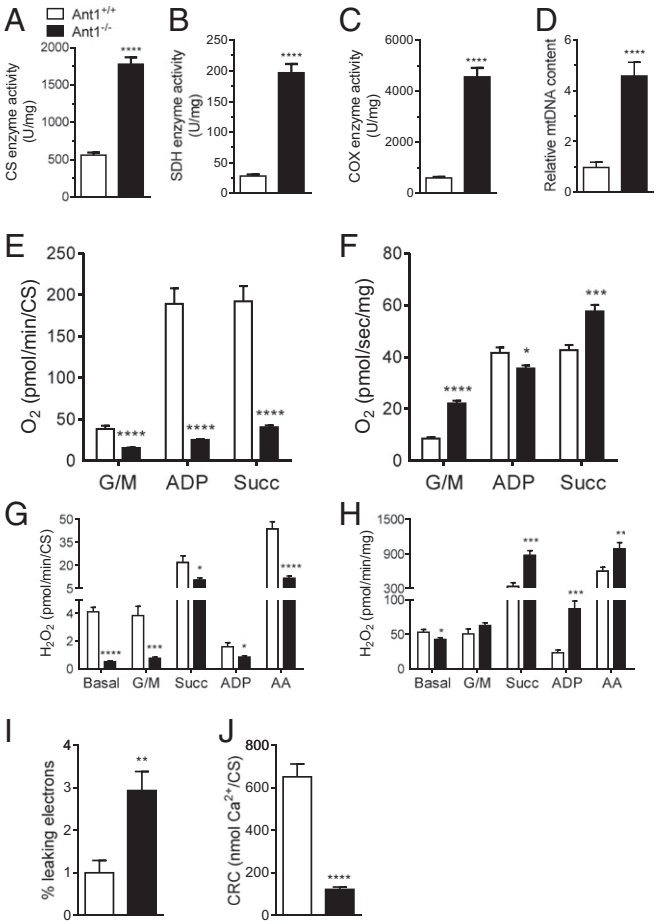

Fig. 4. ANT1 deficiency causes alterations in mitochondrial enzymes and OXPHOS activity. *Ant1*$^{+/+}$ and *Ant1*$^{-/-}$ mice were fed a HFD and killed at 12 mo. Enzyme activity of (*A*) CS, (*B*) SDH, and (*C*) COX in isolated white gastrocnemius muscle expressed as units of activity per wet weight of muscle tissue. (*D*) Relative mtDNA content is represented by fold change of ND1 normalized to B2M in white gastrocnemius and graphed as geometric mean with 95% confidence interval (CI). (*E*) Oxygen consumption in permeabilized muscle fibers from white gastrocnemius per unit of CS enzyme activity. ADP, G/M + ADP; G/M, glutamate + malate; Succ, G/M + ADP + succinate. (*F*) Oxygen consumption in permeabilized white muscle fibers per mg wet weight of muscle tissue. (*G*) H_2O_2 production in permeabilized white muscle fibers per unit of CS enzyme activity. AA = G/M + Succ + ADP + antimycin A; ADP = G/M + Succ + ADP; Basal = no substrates; G/M = glutamate + malate; Succ = G/M + succinate. (*H*) H_2O_2 production in permeabilized white muscle fibers per mg wet weight of muscle tissue. (*I*) Free radical leak in permeabilized white muscle fibers per unit of CS activity expressed as fold change of *Ant1*$^{+/+}$. (*J*) CRC in permeabilized white muscle fibers per unit of CS activity. Data are represented as mean ± SEM; $n = 8$ per group. *$P < 0.05$; **$P < 0.01$; ***$P < 0.001$; ****$P < 0.0001$.

was 47% lower in white fibers, indicating that individual *Ant1*$^{-/-}$ mitochondria release less H_2O_2 (Fig. 4*G* and Fig. S3*I*). By contrast, when H_2O_2 production was normalized to muscle wet weight to reflect whole muscle mitochondrial H_2O_2 production, the white and red muscle fiber H_2O_2 production rates for G/M + Succ + ADP were 2–2.5-fold higher in *Ant1*$^{-/-}$ muscle than *Ant1*$^{+/+}$ muscle (Fig. 4*H* and Fig. S3*J*).

White and red muscle fibers from *Ant1*$^{-/-}$ gastrocnemius also had a three- to fourfold increase in free radical leak during ADP-stimulated respiration (Fig. 4*I* and Fig. S3*K*), free radical leak being an estimate of the proportion of electrons reacting with oxygen to create reactive oxygen species (ROS) (26). Hence, the cumulative muscle ROS production rate is increased in the *Ant1*$^{-/-}$ muscle.

Ant1$^{-/-}$ muscle mitochondria are also acutely sensitive to Ca^{2+} activation of the mitochondrial permeability transition pore (mtPTP) as quantified by the Ca^{2+} retention capacity (CRC) (27). CRC normalized per mitochondrial content was reduced 70–80% for both white and red fibers of the *Ant1*$^{-/-}$ mouse, indicating increased predilection to mitochondrial permeability transition, perhaps the result of the chronically increased muscle ROS production (Fig. 4*J* and Fig. S3*L*).

Induction of FGF21 and GDF15 in Muscle but Not Liver or BAT and No Induction of UCP1. White gastrocnemius muscle RNA sequencing confirmed the absence of ANT1 (*Slc25a4*) mRNA (Fig. 5*A* and Table S1) and revealed the coordinate up-regulation of transcript levels of mitochondrial bioenergetics genes consistent with the hyperproliferation of mitochondria in ANT1-deficient skeletal muscle (Fig. S4*A*). Although the average up-regulation of the nuclear DNA OXPHOS genes is modest, likely due to only some of the nuclear-coded OXPHOS proteins being rate limiting (Fig. 5*B*), the up-regulation of the mtDNA-encoded OXPHOS genes is substantial (Fig. 5*C*). The mtDNA complex IV transcripts are strongly up-regulated, as are the tRNA and rRNA transcripts (Fig. 5*D*).

Consistent with the induction of mitochondrial bioenergetics genes, the mRNA for the transcriptional coactivator for nuclear-coded mitochondrial genes, peroxisome proliferator-activated receptor-γ coactivator (PGC)-1β (*Ppargc1b*), is up-regulated 2.46-fold, although the mRNAs for PGC-1α (*Ppargc1a*) and PGC-1–related coactivator (*Pprc1*) are down-regulated (Table S1). Rip140 (*Nrip1*), an inhibitor of mitochondrial biogenesis (28), is also

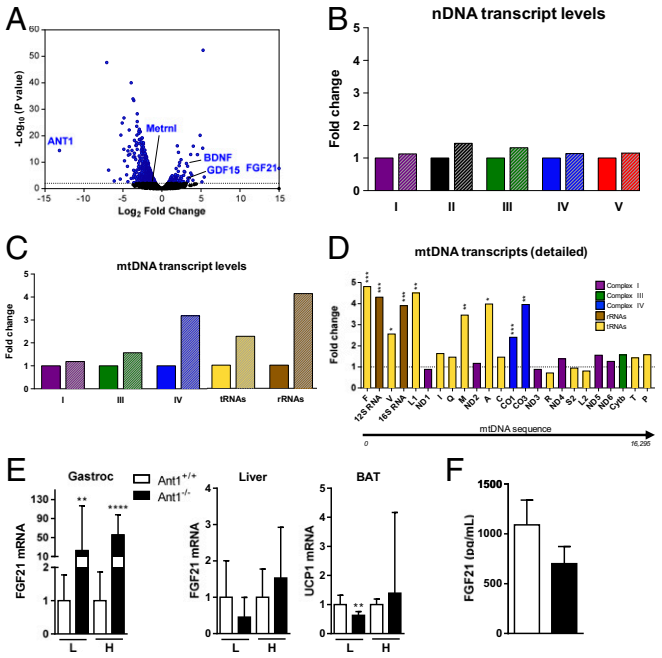

Fig. 5. Alterations in transcript levels of ANT1-deficient gastrocnemius. (*A*) Volcano plot showing distribution of the up- and down-regulated genes in *Ant1*$^{-/-}$ versus *Ant1*$^{+/+}$ white muscle analyzed by RNA sequencing. (*B*) Mean nuclear DNA (nDNA) transcript levels of the electron transport chain complexes. Solid fill, *Ant1*$^{+/+}$; dashed fill, *Ant1*$^{-/-}$. (*C*) mtDNA transcript levels averaged by electron transport chain complexes, transfer RNAs (tRNA), and ribosomal RNAs (rRNA). Solid fill, Ant1$^{+/+}$; dashed fill, Ant1$^{-/-}$. (*D*) mtDNA transcripts shown individually in their sequential order on the mtDNA genome. Data are represented as mean ± SEM; $n = 4$ per group. *$P < 0.01$; **$P < 0.001$; ***$P < 0.0001$. (*E*) Fold change relative levels of FGF21 mRNA in gastrocnemius (gastroc) and liver and UCP1 mRNA in BAT by qPCR. H, HFD; L, LFD. Data are represented as geometric mean with 95% CIs. $n = 4$ per group. **$P < 0.01$; ****$P < 0.0001$. (*F*) Serum FGF21 levels in *Ant1*$^{+/+}$ and *Ant1*$^{-/-}$ mice. $n = 4$ per group.

down-regulated by nearly 50% (Table S1). Additionally, the genes related to apoptosis, cell death, and polyamine metabolism are down-regulated (Fig. S4*B*).

Many transcripts of genes traditionally associated with diabetes are reduced in the *Ant1*$^{-/-}$ white muscle. The mRNAs for insulin receptor substrates (IRS-1 and IRS-2), SHC2, PIK3CA, PDPK1, AKT3, GSK3B, and SGK1 are strongly reduced, as are the AMPK pathway gene transcripts PRKAB2, PRKACB, PRKAG3, and PRKAR1A (Table S1). The mRNAs for the transcriptional regulators FOXO1 and FOS are down-regulated, whereas the FOXO6 transcript level is up-regulated 6.91-fold. The glucose transporter mRNA GLUT1 (*Slc2a1*) is down-regulated, although GLUT4 (*Slc2a4*) is not, even though GLUT1 regulates basal glucose uptake while GLUT4 regulates insulin-mediated glucose uptake. Finally, PPARα (*Ppara*), which is implicated in FGF21 induction in liver (29), is not induced in *Ant1*$^{-/-}$ muscle (Table S1).

Strikingly, the mRNA levels for myokines associated with mitochondrial myopathy and whole body energy homeostasis, FGF21 and GDF15 (15-17), are strongly induced in skeletal muscle (Fig. S4 *C* and *D*). FGF21 transcript is not detected in white gastrocnemius muscle of *Ant1*$^{+/+}$ mice, but it is increased 20–50-fold in *Ant1*$^{-/-}$ mice on a LFD and HFD, respectively (Fig. 5*E* and Fig. S4*C*). GDF15 transcript is also up-regulated in gastrocnemius muscle 4–12-fold on a LFD and HFD, respectively (Fig. S4*D*). By contrast, UCP1 mRNA levels in white gastrocnemius are unchanged (Fig. S4*E*).

Although FGF21 mRNA is strongly induced in *Ant1*$^{-/-}$ muscle (Fig. 5*E*), the level of FGF21 in serum is decreased, not increased (Fig. 5*F*). Moreover, FGF21 mRNA levels were not increased in liver, WAT, or BAT on either LFD or HFD (Fig. 5*E* and Fig. S4*C*). GDF15 mRNA was only increased in WAT on a LFD, not in liver and BAT on LFD, and GDF15 mRNA is down-regulated in BAT and WAT on a HFD (Fig. S4*D*). Finally, *Ucp1* expression was not significantly changed in muscle or BAT on a HFD, decreased in BAT on a LFD, and not significantly increased in liver or WAT on HFD, although expression was highly variable in WAT on a HFD, which could suggest variable beige fat formation (Fig. 5*E* and Fig. S4*E*). BDNF mRNA, which was up-regulated in gastrocnemius muscle, did not change in liver, WAT, or BAT on a HFD (Fig. S4*F*).

Hence, the *Ant1*$^{-/-}$ mouse resistance to a HFD does not appear to be the result of induction of FGF21 in liver, elevated FGF21 in serum, or the induction of *Ucp1* in BAT, as reported for the *PolgA*^{D257A} mutator mouse. Hence, the resistance to a HFD in the *Ant1*$^{-/-}$ mouse appears to be increased substrate oxidation by the high levels of partially uncoupled mitochondria in the skeletal muscle, although increased respiration of WAT might also be a factor.

Discussion

Mice deficient in the heart–muscle–brain ANT isoform, ANT1, are resistant to hyperglycemia, hypersensitive to insulin, and resistant to HFD toxicity. Given that ANT1 deficiency results in reduced ATP/ADP exchange between the mitochondria and the cytosol, this observation might seem contrary to the hypothesis that mitochondrial dysfunction is central to the etiology of diabetes and metabolic syndrome. However, a detailed analysis of the cellular anatomy and physiology of the *Ant1*$^{-/-}$ mouse revealed that ANT1 deficiency is associated with a dramatic compensatory hyperproliferation of partially uncoupled skeletal muscle mitochondria resulting in an overall increase in muscle mitochondrial oxidation of substrates, even in the absence of physical activity.

This protection of *Ant1*$^{-/-}$ mice is not due to increased muscle insulin signaling, as the genes for these pathways are down-regulated. It is also not due to increased BAT hydrolysis of substrates due to the induction by high serum FGF21 or *Ucp1* in BAT, as in the *PolgA*^{D257A} mutator mouse (21), as the *Ant1*$^{-/-}$ mouse serum FGF21 levels were reduced and *Ucp1* is not induced in BAT. Therefore, because the muscle is the primary user of systemic glucose, the glucose tolerance and HFD resistance of the *Ant1*$^{-/-}$ muscle is most likely due to increased muscle mitochondrial respiration, which depletes circulating glucose, nonesterified fatty acids, and triglycerides (30).

In the *PolgA*^{D257A} mutator mouse, FGF21-mediated induction of *Ucp1* with uncoupling of OXPHOS in BAT was proposed to remove the excess calories and account for increased insulin sensitivity and resistance to HFD-induced obesity (21). Because the *PolgA*^{D257A} mutator mouse accumulates abnormally high levels of mtDNA mutations in all tissues (31), increased metabolism of fats and glucose through muscle mitochondrial might also contribute to the glucose tolerance and insulin resistance of the *PolgA*^{D257A} mutator mice, and skeletal muscle mitochondrial function was not analyzed in these animals.

In mice in which *Ucp1* was ectopically expressed in muscle (*Tg-HAS-UCP1*), the partially uncoupled muscle mitochondria are associated with increased insulin sensitivity and resistance to a HFD (32–34). Thus, like the *Ant1*$^{-/-}$ mice, increased muscle mitochondrial respiration in the *Tg-HAS-UCP1* mice rendered them resistant to high glucose and fat toxicity. This supports the notion that increased skeletal muscle mitochondrial respiration due to OXPHOS uncoupling can impart glucose tolerance, insulin sensitivity, and resistance to HFD toxicity.

Therefore, the high glucose tolerance, insulin sensitivity, and resistance to HFD toxicity of the *Ant1*$^{-/-}$ mice is more analogous to that of the *Tg-HAS-UCP1* mice. This similarity is further enhanced, as the knock-out of the *Fgf21* gene in *Tg-HAS-UCP1* mice did not abrogate their tendency to hypoglycemia and increased insulin sensitivity (35).

As the *PolgA*^{D257A}, *Tg-HAS-UCP1*, and *Ant1*$^{-/-}$ mice all impart resistance to hyperglycemia and HFD through uncoupling of OXPHOS in muscle and/or WAT and BAT, then OXPHOS uncoupling must be the basis of their hypoglycemia insulin sensitivity and resistance to HFD. Given that increased mitochondrial respiration protects against excessive substrate toxicity, then the converse should also be true. Impaired mitochondrial OXPHOS should contribute to predisposition to diabetes, obesity, and metabolic syndrome. Modulation of mitochondrial function as an oxidative sink for substrates may thus provide a potential therapeutic strategy for metabolic diseases.

Materials and Methods

Mice. Male *Ant1*$^{-/-}$ and *Ant1*$^{+/+}$ mice (C57BL/6JEiJ) were fed a LFD (13.5% kcal from fat; Purina LabDiet 5001) or a HFD (60% kcal from fat; Purina TestDiet 58G9). Food and water were provided ad libitum. Mice were maintained on a 13:11 h light–dark cycle. All procedures were approved by the Children's Hospital of Philadelphia Institutional Animal Care and Use Committee.

Metabolic Analysis. Body composition was measured by MRI (Echo Medical Systems). Mice were placed in a restraining device and scanned for 90 s. RER and activity were measured over 24 h in metabolic cages (CLAMS; Columbus Instruments) with ad libitum access to food and water.

Glucose Tolerance Test. Mice were fasted overnight for 12 h, and tail blood was collected for glucose and insulin levels. Following i.p. injection of glucose (1.5 g/kg), blood was collected at 20, 40, 60, 90, and 120 min. Glucose was measured using a glucometer (Bayer Ascensia Contour). Insulin was measured from heparinized plasma using an Ultra Sensitive Mouse Insulin ELISA Kit (Crystal Chem).

Electron Microscopy and Immunohistochemistry. For EM studies, gastrocnemius was isolated, and red and white fibers were immediately dissected and fixed with 2.5% (vol/vol) glutaraldehyde, 2.0% (vol/vol) paraformaldehyde in 0.1 M sodium cacodylate buffer, pH 7.4, overnight at 4 °C. For IHC studies, the gastrocnemius, plantaris, and soleus complex was dissected as a whole and frozen in isopentane cooled in liquid nitrogen. Serial cross-sections were immunolabeled for MHC type I, IIa, IIb, and IIx (36).

Mitochondrial Enzyme Activity and mtDNA Content. Red and white gastrocnemius was dissected and frozen in liquid nitrogen. CS enzyme activity was determined by the change in absorbance of DTNB measured at 412 nm. COX enzyme activity was determined by the change in absorbance of reduced cytochrome *c* measured at 550 nm. SDH enzyme activity was determined by the change in absorbance of DCIP measured at 600 nm. Relative mtDNA content was measured by quantitative PCR using primers for ND1 and B2M.

Muscle Fiber Biochemistry. Respiration was performed in saponin permeabilized red and white gastrocnemius muscle fibers using an Oxygraph O2K (Oroboros Instruments) at 37 °C. We added 10 mM glutamate, 5 mM malate, 2 mM ADP, and 10 mM Succ sequentially. ROS production was measured in permeabilized fibers using Amplex Red (ThermoFisher) at 37 °C in a fluorometer. Then, 5 mM glutamate, 5 mM malate, 5 mM Succ, 2 mM ADP, and 10 μM AA were added sequentially. Excitation at 563 nm and emission at 587 nm was measured. CRC was measured in permeabilized fibers using Calcium Green (ThermoFisher) at 37 °C in a fluorometer. Excitation at 505 nm and emission at 535 nm was measured (37).

RNA-Seq and FGF21 and GDF15 Analysis. Total RNA from white gastrocnmeius was extracted with TRIzol and depleted of rRNA using RiboMinus (ThermoFisher). Libraries were prepared with Ion Library kit and sequenced using the Ion Proton Sequencer (ThermoFisher). RNA-seq data were analyzed using Partek Genomics Suite software version 6.12.0109, DESEq. (38), and The Database for Annotation, Visualization and Integrated Discovery v6.7 (DAVID) (39). TrIzol isolated RNA from gastrocnemius, liver, WAT, and BAT was isolated from *Ant1*$^{-/-}$ and *ANT1*$^{+/+}$ mice, and FGF21, GDF15, BDNF, and UCP1 mRNAs were quantifies by TaqMan assay. Serum FGF21 levels were determined by Rat-Mouse FGF21 ELISA Kit (EMD Millipore).

Additional methods are provided in *SI Materials and Methods*.

ACKNOWLEDGMENTS. This work was supported by NIH Grants NS021328, CA182384, OD01944, and DK73691 (to D.C.W.) and University of Pennsylvania Diabetes Research Center Mouse Phenotyping, Physiology, and Metabolism Core Grant P30DK19525.

1. Mootha VK, et al. (2003) PGC-1alpha-responsive genes involved in oxidative phosphorylation are coordinately downregulated in human diabetes. *Nat Genet* 34(3):267–273.
2. Patti ME, et al. (2003) Coordinated reduction of genes of oxidative metabolism in humans with insulin resistance and diabetes: Potential role of PGC1 and NRF1. *Proc Natl Acad Sci USA* 100(14):8466–8471.
3. Lee CH, Olson P, Evans RM (2003) Minireview: Lipid metabolism, metabolic diseases, and peroxisome proliferator-activated receptors. *Endocrinology* 144(6):2201–2207.
4. Petersen KF, Dufour S, Befroy D, Garcia R, Shulman GI (2004) Impaired mitochondrial activity in the insulin-resistant offspring of patients with type 2 diabetes. *N Engl J Med* 350(7):664–671.
5. Ritov VB, et al. (2005) Deficiency of subsarcolemmal mitochondria in obesity and type 2 diabetes. *Diabetes* 54(1):8–14.
6. Kelley DE, He J, Menshikova EV, Ritov VB (2002) Dysfunction of mitochondria in human skeletal muscle in type 2 diabetes. *Diabetes* 51(10):2944–2950.
7. Boushel R, et al. (2007) Patients with type 2 diabetes have normal mitochondrial function in skeletal muscle. *Diabetologia* 50(4):790–796.
8. Mogensen M, et al. (2007) Mitochondrial respiration is decreased in skeletal muscle of patients with type 2 diabetes. *Diabetes* 56(6):1592–1599.
9. Savage DB, Petersen KF, Shulman GI (2007) Disordered lipid metabolism and the pathogenesis of insulin resistance. *Physiol Rev* 87(2):507–520.
10. Koves TR, et al. (2008) Mitochondrial overload and incomplete fatty acid oxidation contribute to skeletal muscle insulin resistance. *Cell Metab* 7(1):45–56.
11. Ballinger SW, et al. (1992) Maternally transmitted diabetes and deafness associated with a 10.4 kb mitochondrial DNA deletion. *Nat Genet* 1(1):11–15.
12. Ballinger SW, Shoffner JM, Gebhart S, Koontz DA, Wallace DC (1994) Mitochondrial diabetes revisited. *Nat Genet* 7(4):458–459.
13. van den Ouweland JM, et al. (1994) Maternally inherited diabetes and deafness is a distinct subtype of diabetes and associates with a single point mutation in the mitochondrial tRNA($^{Leu(UUR)}$) gene. *Diabetes* 43(6):746–751.
14. Wilson FH, et al. (2004) A cluster of metabolic defects caused by mutation in a mitochondrial tRNA. *Science* 306(5699):1190–1194.
15. Tyynismaa H, et al. (2010) Mitochondrial myopathy induces a starvation-like response. *Hum Mol Genet* 19(20):3948–3958.
16. Suomalainen A, et al. (2011) FGF-21 as a biomarker for muscle-manifesting mitochondrial respiratory chain deficiencies: A diagnostic study. *Lancet Neurol* 10(9): 806–818.
17. Yatsuga S, et al. (2015) Growth differentiation factor 15 as a useful biomarker for mitochondrial disorders. *Ann Neurol* 78(5):814–823.
18. Chavez AO, et al. (2009) Circulating fibroblast growth factor-21 is elevated in impaired glucose tolerance and type 2 diabetes and correlates with muscle and hepatic insulin resistance. *Diabetes Care* 32(8):1542–1546.
19. Shin MY, et al. (2016) Association between growth differentiation factor 15 (GDF15) and cardiovascular risk in patients with newly diagnosed type 2 diabetes mellitus. *J Korean Med Sci* 31(9):1413–1418.
20. Nies VJ, et al. (2016) Fibroblast growth factor signaling in metabolic regulation. *Front Endocrinol (Lausanne)* 6:193.
21. Wall CE, et al. (2015) High-fat diet and FGF21 cooperatively promote aerobic thermogenesis in mtDNA mutator mice. *Proc Natl Acad Sci USA* 112(28):8714–8719.
22. Levy SE, Chen YS, Graham BH, Wallace DC (2000) Expression and sequence analysis of the mouse adenine nucleotide translocase 1 and 2 genes. *Gene* 254(1-2):57–66.
23. Graham BH, et al. (1997) A mouse model for mitochondrial myopathy and cardiomyopathy resulting from a deficiency in the heart/muscle isoform of the adenine nucleotide translocator. *Nat Genet* 16(3):226–234.
24. Esposito LA, Melov S, Panov A, Cottrell BA, Wallace DC (1999) Mitochondrial disease in mouse results in increased oxidative stress. *Proc Natl Acad Sci USA* 96(9):4820–4825.
25. Lin J, et al. (2002) Transcriptional co-activator PGC-1 alpha drives the formation of slow-twitch muscle fibres. *Nature* 418(6899):797–801.
26. Sanz A, et al. (2006) Methionine restriction decreases mitochondrial oxygen radical generation and leak as well as oxidative damage to mitochondrial DNA and proteins. *FASEB J* 20(8):1064–1073.
27. Kokoszka JE, et al. (2004) The ADP/ATP translocator is not essential for the mitochondrial permeability transition pore. *Nature* 427(6973):461–465.
28. Seth A, et al. (2007) The transcriptional corepressor RIP140 regulates oxidative metabolism in skeletal muscle. *Cell Metab* 6(3):236–245.
29. Inagaki T, et al. (2007) Endocrine regulation of the fasting response by PPARalpha-mediated induction of fibroblast growth factor 21. *Cell Metab* 5(6):415–425.
30. Picard M, et al. (2015) Mitochondrial functions modulate the stress response in mice. *Psychoneuroendocrinology* 61:74.
31. Trifunovic A, et al. (2004) Premature ageing in mice expressing defective mitochondrial DNA polymerase. *Nature* 429(6990):417–423.
32. Klaus S, Rudolph B, Dohrmann C, Wehr R (2005) Expression of uncoupling protein 1 in skeletal muscle decreases muscle energy efficiency and affects thermoregulation and substrate oxidation. *Physiol Genomics* 21(2):193–200.
33. Neschen S, et al. (2008) Uncoupling protein 1 expression in murine skeletal muscle increases AMPK activation, glucose turnover, and insulin sensitivity in vivo. *Physiol Genomics* 33(3):333–340.
34. Keipert S, Voigt A, Klaus S (2011) Dietary effects on body composition, glucose metabolism, and longevity are modulated by skeletal muscle mitochondrial uncoupling in mice. *Aging Cell* 10(1):122–136.
35. Ost M, et al. (2015) Muscle mitochondrial stress adaptation operates independently of endogenous FGF21 action. *Mol Metab* 5(2):79–90.
36. Gouspillou G, et al. (2014) The relationship between muscle fiber type-specific PGC-1α content and mitochondrial content varies between rodent models and humans. *PLoS One* 9(8):e103044.
37. Picard M, et al. (2008) Resistance to Ca2+-induced opening of the permeability transition pore differs in mitochondria from glycolytic and oxidative muscles. *Am J Physiol Regul Integr Comp Physiol* 295(2):R659–R668.
38. Anders S, Huber W (2010) Differential expression analysis for sequence count data. *Genome Biol* 11(10):R106.
39. Huang W, Sherman BT, Lempicki RA (2009) Systematic and integrative analysis of large gene lists using DAVID bioinformatics resources. *Nat Protoc* 4(1):44–57.